Supplementary Information

Azole-carboxylate-modulated assembly of $[Mo_2O_2S_2]^{2+}$ units: structural evolution from $\{Mo_{12}\}$ to $\{Mo_{16}\}$ rings for enhanced proton conductivity

Huachao Liu‡[a], Rongqing Tang‡[a], Yubin Ma[a], Zhiyu Shao*[a], and Weimin Xuan*[a]

[a]State Key Laboratory of Advanced Fiber Materials& College of Chemistry and Chemical Engineering, Donghua University, Shanghai 201620, P R China
E-mail: zyshao@dhu.edu.cn, weiminxuan@dhu.edu.cn

‡H. Liu and R. Tang contributed equally.

Contents

1. Materials

All obtained reagents, including 1,4-bis(imidazol-1-yl)terephthalic acid (H_2BTA) and 2,5-bis(1,2,4-triazol-1-yl) terephthalic acid (H_2TTPA), $(NH_4)_6Mo_7O_{24}\cdot 4H_2O$, KOH were all commercially available and were purified without further purification. Oxothio dimer $[Mo_2S_2O_2(H_2O)_6]^{2+}$ was synthesized according to the literature[1].

2. Instrumentation

Crystallography: Single-crystal XRD data of compounds **1** and **2** were collected at 150 K on a diffractometer equipped with a HyPix-Arc 150 curved detector and an XtaLAB Synergy Custom detector. All non-hydrogen atoms are anisotropically refined by the least square method except for the guest water molecules. CCDC-2537570 (**1**), CCDC-2537571 (**2**), contain the supplementary crystallographic data for this paper. These data can be obtained free of charge via www.ccdc.cam.ac.uk/data_request/cif.

Element Analyses: Element analyses were determined by VARIDEL III Elemental Analyzer.

Inductively Coupled Plasma Optical Emission Spectroscopy (ICP-OES): Elemental analyses for Mo, Na and K were determined with a Leeman Prodigy Plus inductivity-coupled plasma Inductively Coupled Plasma Optical Emission Spectroscopy (ICP-OES).

Thermogravimetric Analysis (TGA): Thermogravimetric analysis was performed on a METTLER TOLEDO TG8000 Thermogravimetric Analyzer under nitrogen flow at a typical heating rate of 10 °C·min^{-1}.

Powder X-ray Diffraction (PXRD): The powder X-ray diffraction (PXRD) pattern was collected on a D8 ADVANCE instrument (Bruker, Germany) using Cu Kα radiation. Data were acquired over a 2θ range of 5° to 50° at a scanning rate of 5°/min.

Water adsorption: Water isotherms were measured on a Micromeritics 3Flex, and the water uptake in g g^{-1} units was calculated as [(adsorbed amount of water)/ (amount of water)]. Prior to the water adsorption measurements, water (analyte) was flash frozen under liquid nitrogen and then evacuated under dynamic vacuum at least three times to remove any gases in the water reservoir. The P_0 was checked at room temperature before measurement. The measurement temperature was controlled using a Micromeritics temperature controller.

Proton conductivity characterization: The samples for proton conductivity measurements were prepared as follows. The pure-phase crystals of compound **1** and compound **2** were ground into fine powders, and approximately 50 mg of the homogeneous powder was loaded into a die with a diameter of 5 mm (area = 0.196 cm^2). The powders were then pressed under a pressure of 10 MPa for 10 min to form pellets with a thickness of about 0.12 cm. Electrochemical AC impedance measurements were carried out on a CHI760E electrochemical workstation. The measurement parameters were set as follows: a frequency range of 0.1 Hz to 10^6 Hz and an AC voltage amplitude of 50 mV. The resulting Nyquist plots were obtained by fitting the impedance data to an equivalent circuit using ZView2 software. The proton conductivity (σ) was calculated according to the following equation:

$$\sigma = \frac{L}{SR}$$

In the equation, σ represents the proton conductivity ($S \cdot cm^{-1}$), L is the thickness of the sample (cm), S denotes the surface area of the sample (cm^2), and R is the resistance obtained from the impedance measurement (Ω). In addition, the corresponding activation energy can be calculated from the proton conductivity values measured at different temperatures, according to the following equation:

$$\sigma_T = \sigma_0 exp(\frac{-E_a}{k_B T})$$

Here, T is the temperature (K), σ_0 denotes the pre-exponential factor, E_a is the activation

energy (eV), and k_B is the Boltzmann constant. Proton conduction in hydrated systems mainly follows two mechanisms, namely the Vehicle mechanism and the Grotthuss mechanism. The Vehicle mechanism is characterized by the translational motion of hydrated protons and is associated with relatively high activation energies (E_a> 0.4 eV). In contrast, the Grotthuss mechanism involves proton hopping through the reorganization of hydrogen-bond networks, exhibiting lower activation energies (E_a> 0.4 eV) and higher diffusion efficiency. Accordingly, the activation energy values obtained can serve as an important criterion for distinguishing between different proton conduction mechanisms[2,3].

3. Synthesis

Synthesis of $H_4BTA\{(Mo_2O_2S_2)_6(OH)_{12}(H_2O)_2BTA\}\cdot 19H_2O$ (1)

The 1,4-bis(imidazol-1-yl)terephthalic acid (H_2BTA) (8mg, 0.027mmol) was dissolved in 1 mL of water under stirring. $[Mo_2O_2S_2]^{2+}$(aq) (0.74 mL) was added, and the mixture was stirred for 30 min. The pH was adjusted to 4.5 using 4 M KOH, immediately resulting in the formation of a yellow precipitate. After stirring for an additional 30 min, the mixture was transferred to a glass vial, sealed, and heated in an oven at 100 °C for 6 h. Upon cooling, yellow crystals formed at the bottom of the vial. The product was collected, washed with water, and dried. (yield 23% based on Mo). Element analyses (%) calcd for $C_{28}H_{77}Mo_{12}N_8O_{53}S_{12}$; H, 2.67, C, 11.56, N, 3.85, S, 13.22, Mo, 39.57; Found: H, 2.60, C, 12.07, N, 3.90, S, 13.25, Mo, 39.34. FTIR (cm^{-1}): 1582 (s), 1417 (m), 1112 (w), 1047 (m), 962 (s), 642 (m), 507 (s) and 571 (w).

Synthesis of $K_9H\{(Mo_2O_2S_2)_8O_8(OH)_8(H_2O)_4TTPA\}\cdot 55H_2O$ (2)

The 2,5-bis(1,2,4-triazol-1-yl) terephthalic acid (H_2TTPA) (5mg, 0.017mmol) was dissolved in 4 mL of water under stirring. $[Mo_2O_2S_2]^{2+}$ (1 mL) was added, and the mixture was stirred for 10 min. The pH was adjusted to 4.5 using 1 M KOH, followed by heating at 50 °C with continuous stirring for 1 h. After cooling to room temperature, the mixture was filtered, and the filtrate was allowed to slowly evaporate at ambient temperature for 10 days, yielding orange-red block-shaped crystals. The product was collected, washed with water, and dried to afford the final compound. (yield 31% based on Mo). Element analyses (%) calcd for $C_{12}H_{133}K_9Mo_{16}N_6O_{95}S_{16}$; H, 3.13, C, 3.37, N, 1.96, S, 11.89, Mo, 35.85, K, 8.22, O, 35.50; Found: H, 3.08, C, 3.45, N, 2.01, S, 11.74, Mo, 35.47, K, 8.18, O, 35.39. FTIR (cm^{-1}): 1617 (m), 1387 (m), 1207 (w), 1132 (m), 1077 (w), 967 (s), 652 (w) and 508 (s).

A systematic screening over a pH range of 3.50 to 5.50 revealed that the solution pH is crucial for the successful synthesis of compounds 1 and 2. In the lower pH range of 3.50 to 4.00, the reaction mixtures mostly remained as clear orange or orange yellow solutions. While a few crystals began to appear at pH 4.25, both systems successfully yielded a large quantity of high quality single crystals exclusively at pH 4.50. When the pH was further increased from 4.75 to

5.50, large amounts of yellow precipitates were rapidly generated instead of the desired single crystals. Therefore, maintaining a precise pH of 4.50 is essential for the successful crystallization of the target compounds.

4. Crystallographic data and crystal structures of compound 1 and 2

Table S1. Crystallographic data for compound **1** and **2**.

Complex	**1**	**2**
Formula	$C_{28}H_{77}Mo_{12}N_8O_{53}S_{12}$	$C_{12}H_{133}K_9Mo_{16}N_6O_{95}S_{16}$
Formula weight	2910.05	4282.19
Temperature (K)	170.00	150.00
Crystal system	Triclinic	Trigonal
Space group	*P-1*	*R-3*
a/Å	9.6711(4)	42.1527(7)
b/Å	14.2667(5)	42.1527(7)
c/Å	16.4303(7)	17.1567(3)
***α*(°)**	70.022(3)	90°
***β*(°)**	73.351(4)	90°
***γ*(°)**	87.078(3)	120°
V/Å^3	2038.46(15)	26400.7(10)
Z	1	9
D_c**(g/cm^3)**	2.342	2.128
F(000)	1398.0	16332.0
Reflections collected	25494	50937
Independent reflections	8108 [$R_{(int)}$ = 0.0382]	11488 [$R_{(int)}$ = 0.0571]
GOF	1.073	1.047
Final R indices [I>2sigma(I)]	R_1 = 0.0392, wR_2 = 0.1054	R_1 = 0.0866, wR_2 = 0.2563
R indices (all data)	R_1 = 0.0404, wR_2 = 0.1062	R_1 = 0.1008, wR_2 = 0.2682

$^aR_1 = \Sigma||F_o| - |F_c||/\Sigma|F_o|$, $^bwR_2 = [\Sigma w(F_o^2 - F_c^2)^2/\Sigma w(F_o^2)^2]^{1/2}$

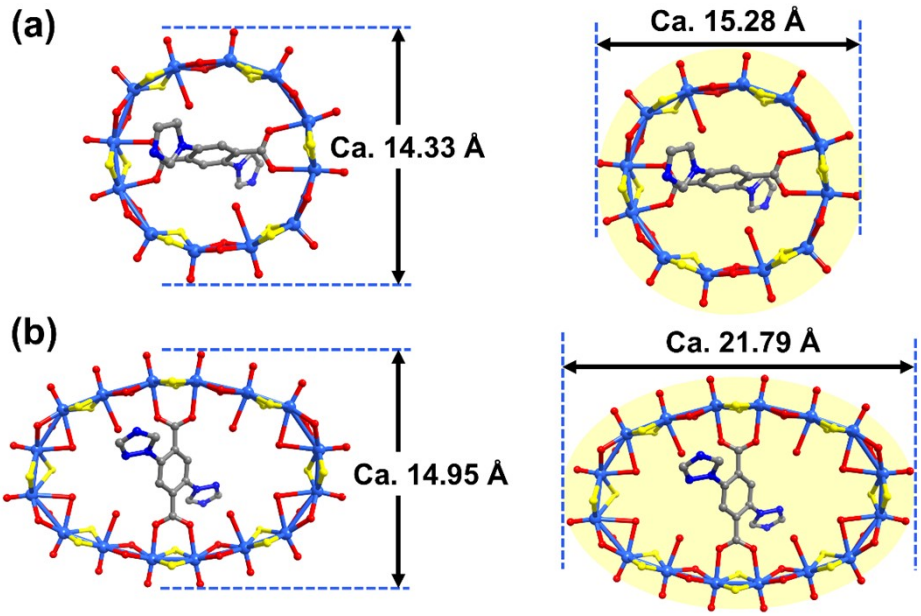

Fig. S1 Comparison of the dimensions and shapes of the host frameworks: (a) length and width of the {Mo_{12}} macrocycle in **1**, exhibiting a near-perfect circular profile; (b) length and width of the {Mo_{16}} macrocycle in **2**, displaying pronounced lateral elongation that results in an elliptical outline. Colour code: Mo, blue; C, grey; N, dark blue; S, yellow; O, red. H atoms are omitted for clarity.

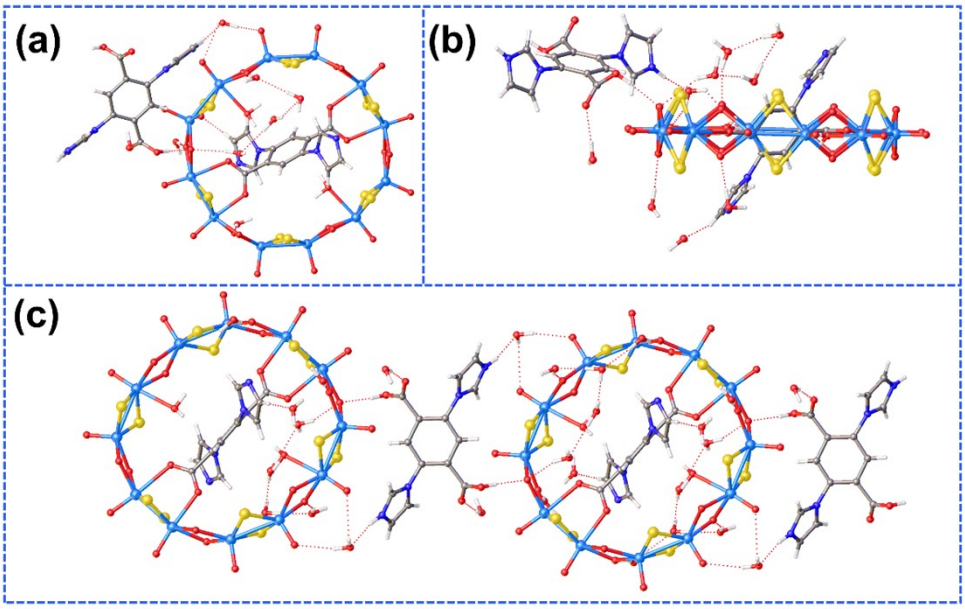

Fig. S2 The hydrogen bonding interactions of compound **1** were visualized using crystallographic software. (a) and (b) illustrate the intramolecular hydrogen bonds from different perspectives, while (c) displays the intermolecular hydrogen bonding interactions.

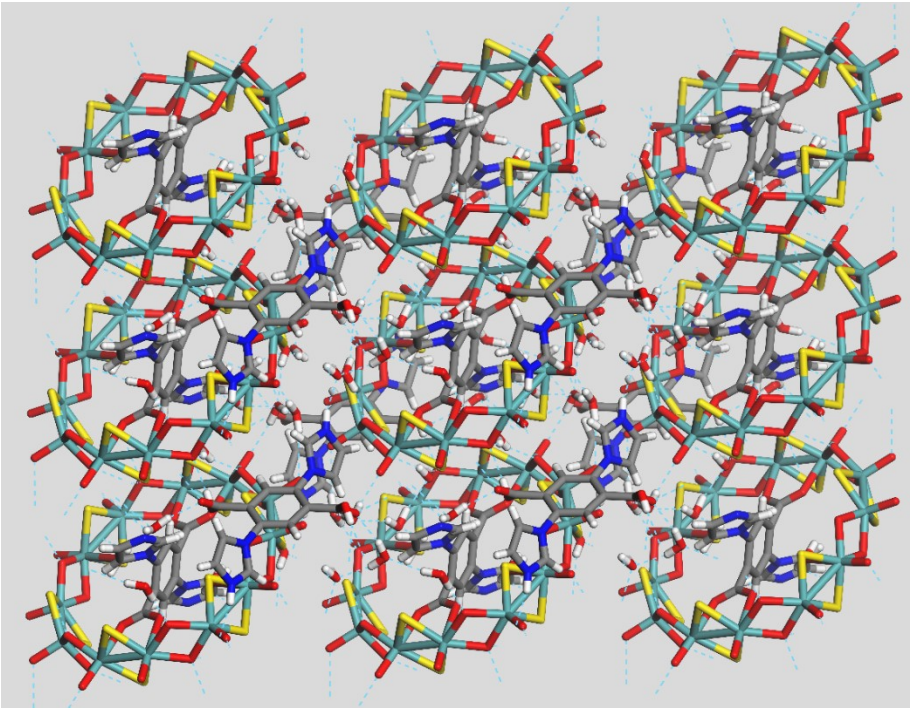

Fig. S3 The dense network of compound **1** packed via intermolecular hydrogen-bonding interactions. Color code: Mo, dark green; O, red; S, yellow; C, gray; N, deep blue; H, white.

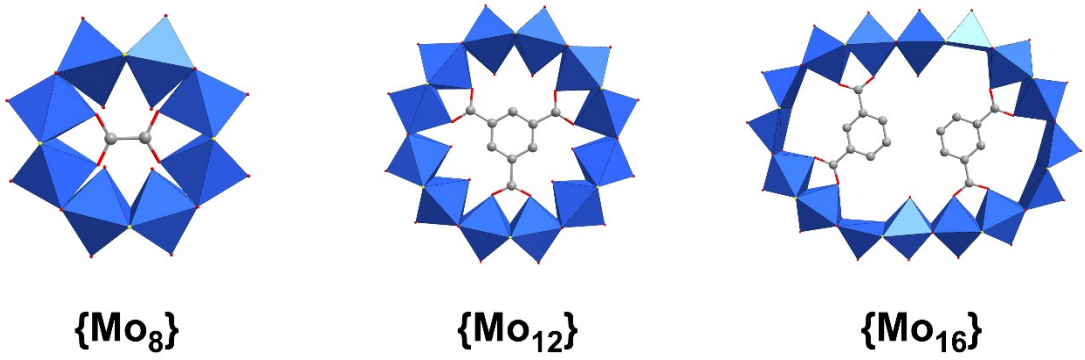

Fig. S4 Several previously reported macrocycles based on $[Mo_2O_2S_2]^{2+}$ building blocks are presented, all of which are characterized by the complete encapsulation of a central template within the Mo-S macrocyclic host. The central carboxylic acid templates employed are oxalic acid, trimesic acid, and isophthalic acid, respectively.[4-7]

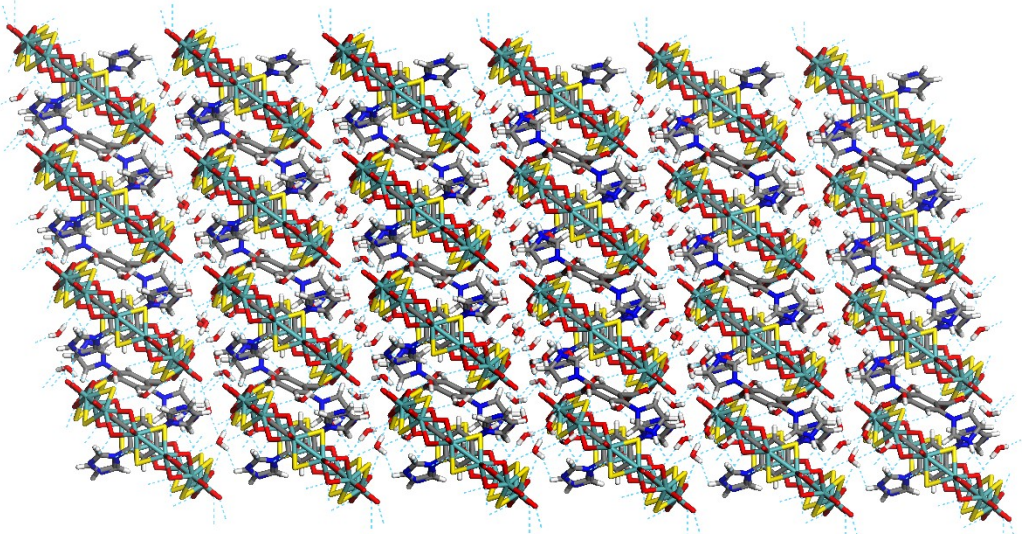

Fig. S5 The well-ordered and tightly packed framework of Compound **1**, constructed via hydrogen-bonding interactions, exhibits a near absence of internal voids.

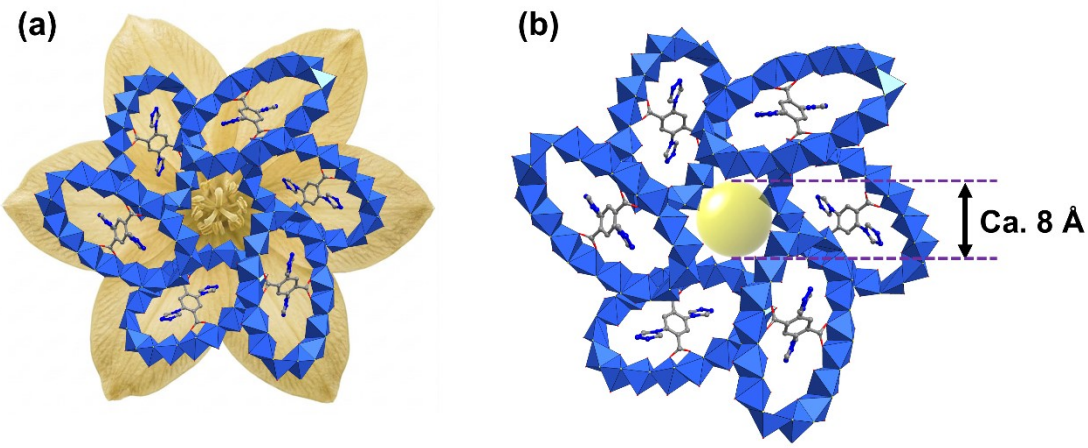

Fig. S6 Molecular packing diagrams of compound **2**: (a) view of the packing via electrostatic interactions into an open framework with a local petal-like arrangement, (b) showcasing a pore diameter of approximately 8 Å. For clarity, free water molecules and countercations have been omitted.

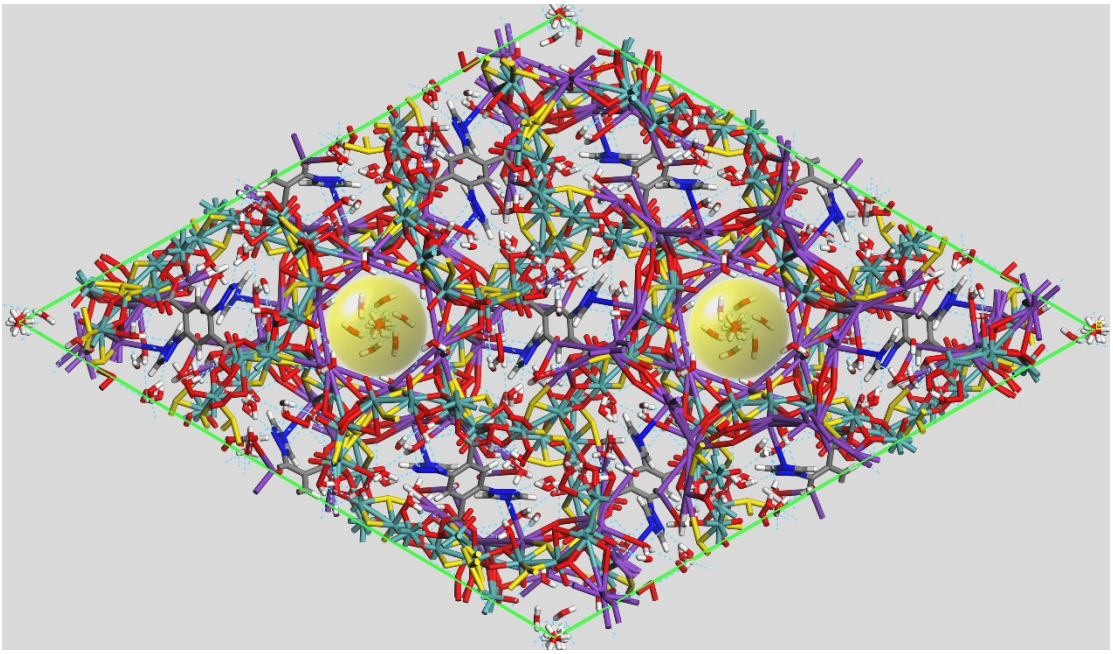

Fig. S7 The framework of compound **2**, assembled via electrostatic and hydrogen-bonding interactions, accommodates counter-cations and guest water molecules within its channels.

5. PXRD spectra of compound 1 and 2

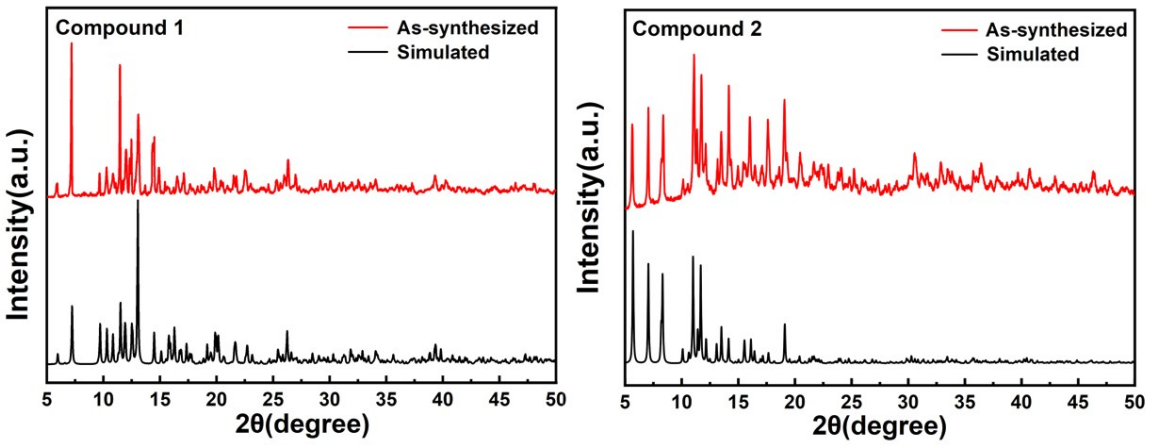

Fig. S8 Experimental and simulated PXRD patterns of compounds **1** and **2**.

The experimental PXRD patterns of **1** and **2** match well with their respective simulated patterns, confirming the bulk phase purity.

6. TGA results of compound 1 and 2

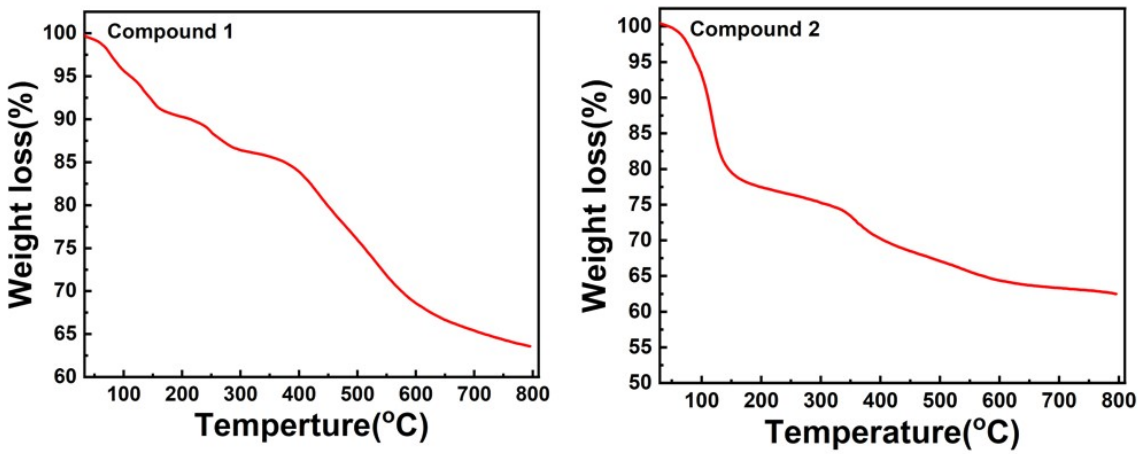

Fig. S9 TGA curves of compounds **1** (left) and **2** (right).

The first weight loss stage up to 200 °C corresponds to the dehydration of 19 and 55 water molecules for **1** and **2**, respectively.

7. FT-IR spectra of compound 1 and 2

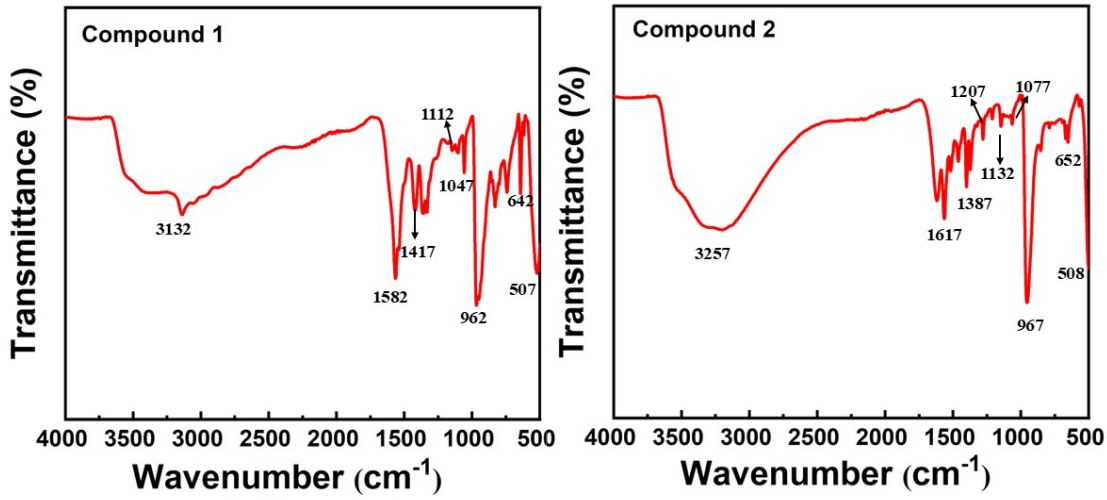

Fig. S10 FT-IR spectra of compound **1** and **2**.

In compound **1**, the absorption bands observed at 507, 642, and 962 cm^{-1} are assigned to the ν(Mo-S-Mo), ν(Mo-OH-Mo), and ν(Mo=O) stretching vibrations, respectively. The absorption peaks at 1047 cm^{-1}, 1112 cm^{-1}, and 1417 cm^{-1} are attributed to the stretching vibrations of C=C, C=N, and C–N bonds in the azole ligands. The bands at 1582 cm^{-1} and 3132 cm^{-1} are associated with the bending and stretching vibrations of hydroxyl groups, respectively. Similarly, for **2**, the absorption bands at 508 cm^{-1}, 652 cm^{-1}, and 967 cm^{-1} are assigned to the ν(Mo-S-Mo), ν(Mo-OH-Mo), and ν(Mo=O) stretching vibrations. The absorption peaks at 1077 cm^{-1}, 1132 cm^{-1}, 1207 cm^{-1}, and 1387 cm^{-1} correspond to the stretching vibrations of C=C, C=N, C–N, and N–N bonds in the azole ligands. The bands appearing at 1617 cm^{-1} and 3257 cm^{-1} are attributed to the bending and stretching vibrations of hydroxyl groups, respectively[8,9].

8. Equivalent Circuit for Impedance Fitting

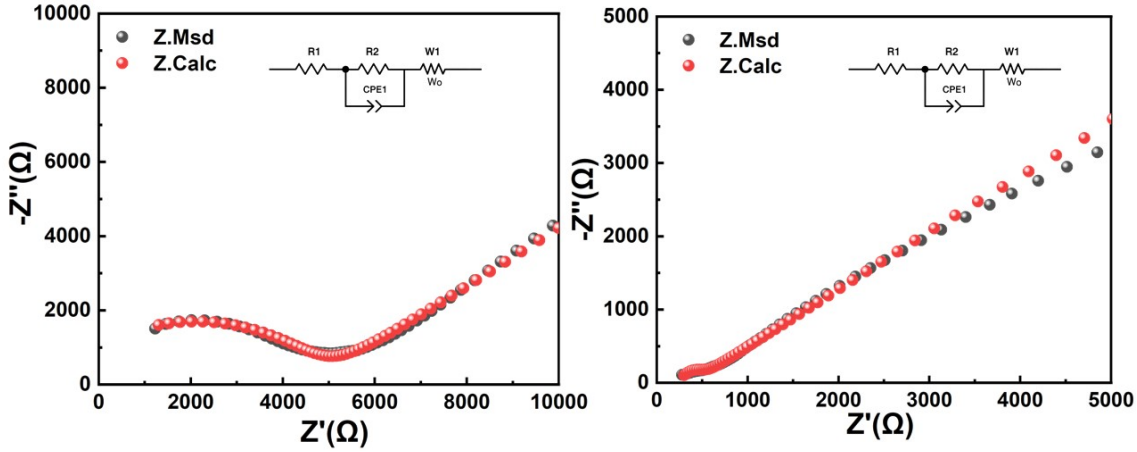

Fig. S11 The resistance value of compound **1** and **2** could be obtained by fitting the curves using ZView2.

The equivalent circuit was used to fit the impedance spectra. *Z.Msd* is the test plot (black) and *Z.Calc* is the fitting plot (red). *C* is capacitive processes, *R* is the resistance of the sample and W_o is the Warburg diffusion term associated with the electrode reactions.

9. Proton Conduction Results of compound 1 and 2

Table S2. Resistance (R) and proton conductivity (σ) of compound **1** under different relative humidities.

RH (%)	R (Ω)	σ (S cm^{-1})
53	1.75×10^{9}	3.49×10^{-10}
68	4.05×10^{8}	3.09×10^{-9}
75	1.60×10^{8}	7.80×10^{-9}
85	4.20×10^{6}	2.98×10^{-7}
98	4.71×10^{4}	1.30×10^{-5}

Table S3. Resistance (R) and proton conductivity (σ) of compound **2** under different relative humidities.

RH (%)	R (Ω)	σ (S cm^{-1})
53	5.12×10^{4}	1.20×10^{-5}
68	4.04×10^{4}	1.53×10^{-5}
75	3.70×10^{4}	1.66×10^{-5}
85	1.47×10^{4}	4.20×10^{-5}
98	1.23×10^{3}	4.98×10^{-4}

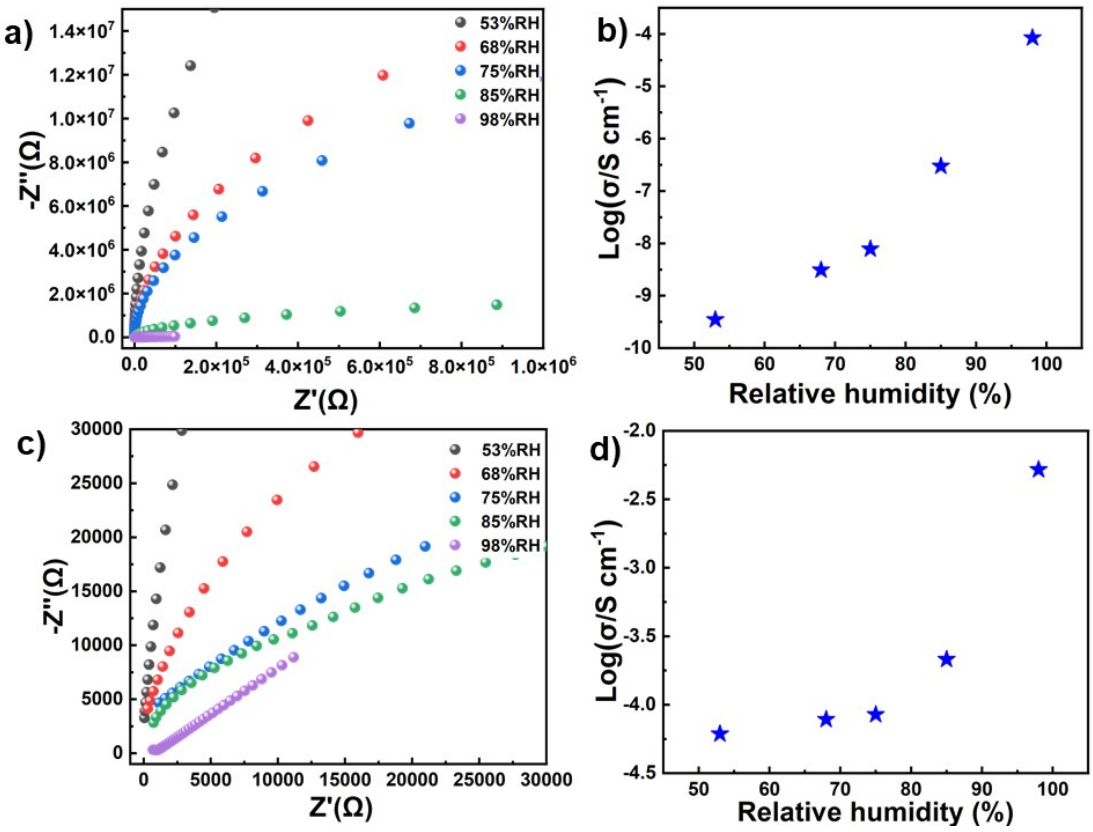

Fig.S12 Proton conductivity measurements of compounds **1** and **2**: (a) Nyquist curves at 30 ℃ and various RHs of **1**; (b) humidity-dependent proton conductivity at 30℃ of **1**; (c) Nyquist curves at 30℃ and various RHs of **2**; (d) humidity-dependent proton conductivity at 30 ℃ of **2**.

Table S4 Resistance (R) and proton conductivity (σ) of compound **1** at different temperatures under 98% RH.

T(℃)	*R* (Ω)	*σ* (S cm^{-1})
30	47256	1.30×10^{-5}
40	25125	2.44×10^{-5}
50	6887	8.89×10^{-5}
60	4347	1.41×10^{-4}
70	3170	1.93×10^{-4}
80	2763	2.22×10^{-4}
90	1560	3.92×10^{-4}

Table S5 Resistance (R) and proton conductivity (σ) of compound **2** at different temperatures under 98% RH.

***T*(℃)**	***R* (Ω)**	***σ* (S cm^{-1})**
30	1229	4.98×10^{-4}
40	756	1.73×10^{-3}
50	335	1.94×10^{-3}
60	302	2.03×10^{-3}
70	259	2.36×10^{-3}
80	189	3.44×10^{-3}
90	135	4.53×10^{-3}

10. Water adsorption–desorption isotherms of compound 1 and 2

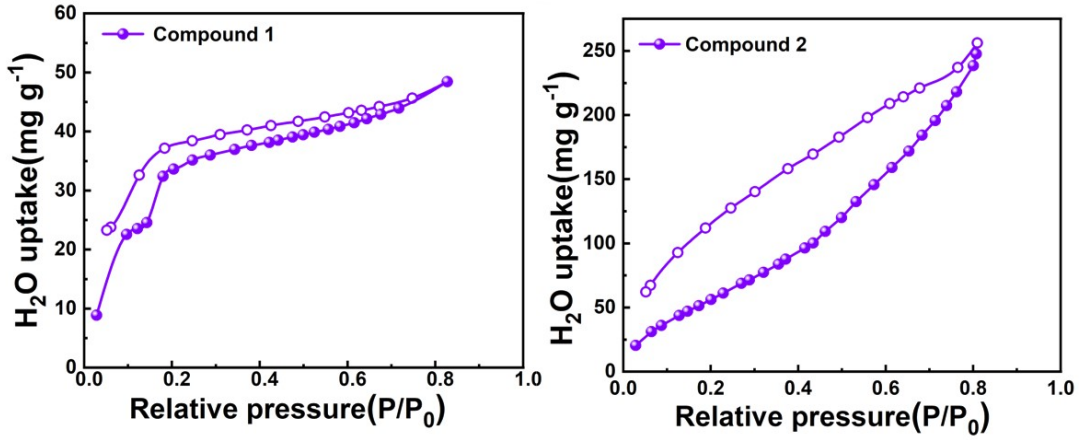

Fig.S13 Water vapor adsorption-desorption isotherms of compounds **1** and **2**.

11. Current–Time Relationship in the Hebb–Wagner Polarization Test

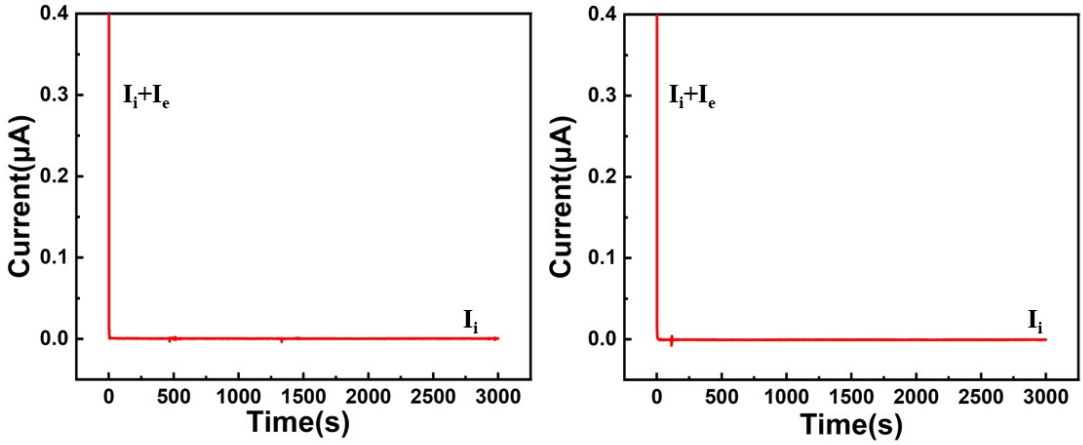

Fig. S14 Time-current relationship plots of compounds **1** and **2** in the Hebb-Wagner polarization method.

The results indicate that both materials exhibit proton conduction rather than electronic conduction. The applied voltage is 3 V and the DC current stabilized at 7.13×10^{-5} μA and 6.25×10^{-4} μA. The applied voltage and the measured DC current were substituted into the equation $R = U/(I\ R)$ to obtain the corresponding resistance values. The calculated resistance (R) was then used to determine the electronic conductivity according to the equation $\sigma = L/(S\ R)$ The samples used for electronic conductivity measurements were prepared following the same procedure as those for proton conductivity measurements. Additionally, the thickness (L) and surface area (S) of the samples were identical to those used in the proton conductivity measurements. After

calculation, the electronic conductivities of the two compounds were determined to be 1.15×10^{-10} S cm^{-1} and 1.28×10^{-10} S cm^{-1}, respectively.

12. Proton Transport Pathways in compounds 1 and 2

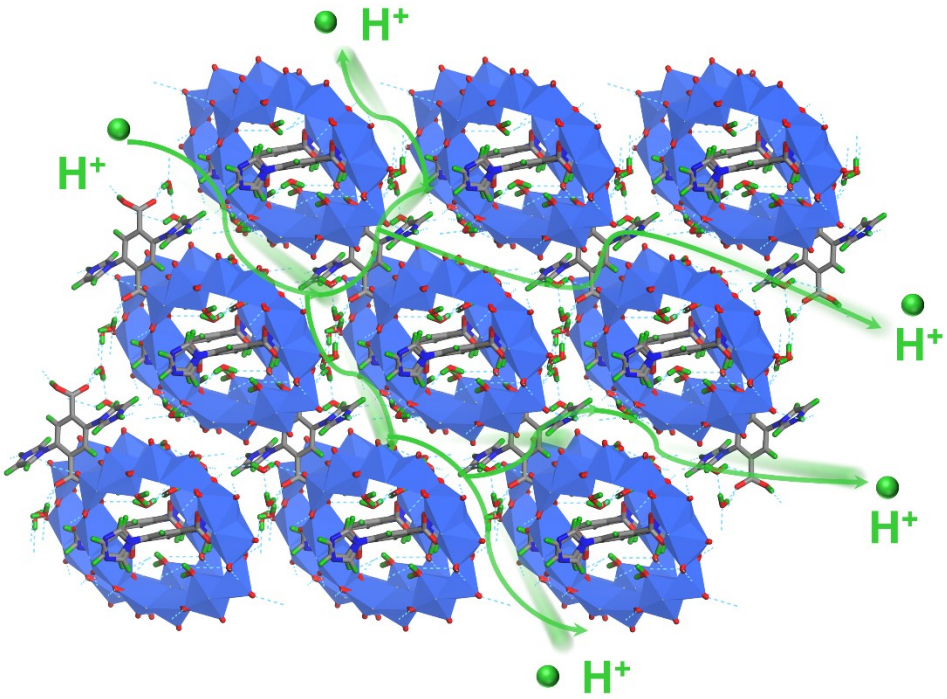

Fig. S15 Proposed Potential Pathways for Proton Transport Based on the Structural Features of Compound **1**. Hydrogen atoms are represented as green spheres for clarity.

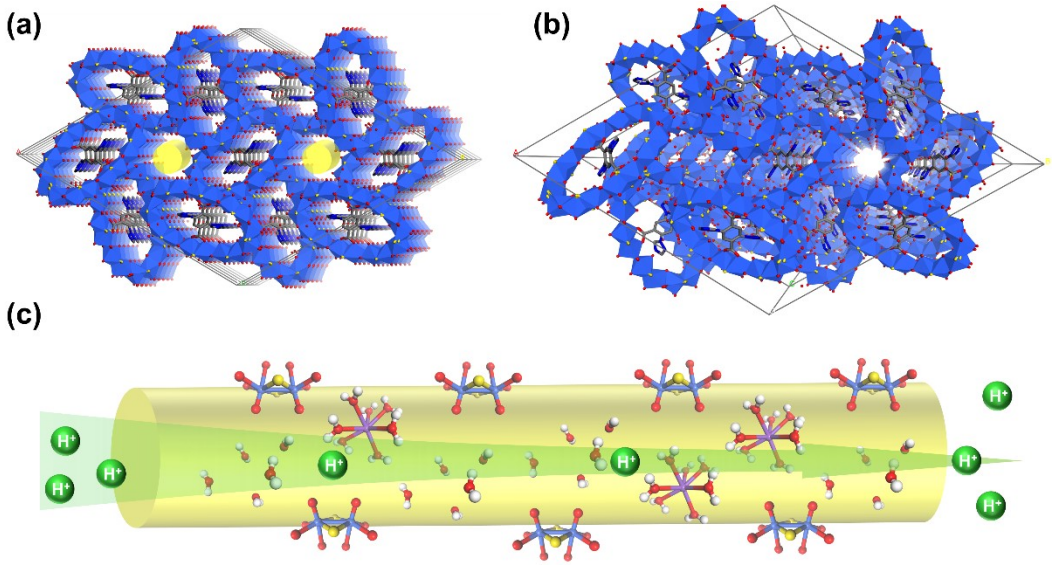

Fig. S16 (a-b) Views of the channels within the packing framework of Compound **2** from different perspectives (free water molecules and counter-cations in the channels are omitted for clarity). (c) Potential proton transport pathways are illustrated; the

channels accommodate protons, free water molecules, K^+ ions and partial terminal oxygen atoms of the $\{Mo_{16}\}$ macrocyclic hosts, which together construct a dense hydrogen-bonding network.

13.Water Vapor Adsorption Capacity of Representative POM-Based Conductors

Table S6 Comparison of water uptake and proton conductivity for representative POM-based crystalline materials.*

Compound	H_2O vapor adsorption capacity (mg/g)	P/P_0	Ref
$\{Mo_{12}\}$	**48.44**	**0.82**	**This work**
$\{Mo_{16}\}$	**256.14**	**0.82**	
$((NH_4)_{21}H^+_{59-2x}[Mo^V_{180}Mo^{VI}_{60}(OH)_{60}O_{620-x}(SO_3)_{20-x}(SO_4)_x]\cdot ca.337\ H_2O$	170.28	0.99	10
$\{[Cu(en)_2]@\{[Cu_2(en)_2(trz)_2]_6(Nb_{68}O_{188})\}\}$	175.90	0.78	11
$Na_{22}H_{30}\{Mo_{132}O_{372}(OH)_{10}(H_2O)_{12}(SO_4)_5(CH_3COO)_{20}\}\cdot 122H_2O$	129.23	0.99	12
$Na_3H_6\{Ce_{11}Mo_{96}O_{286}(H_2O)_{101}(SO_4)_8\}\cdot 170H_2O$	250.92	0.99	
$\{[Mn_6Mo_6O_{37}]La_3[MnMo_6O_{24}]\}$	165.43	0.96	13
$\{[Mn_6Mo_6O_{37}]Pr_3[MnMo_6O_{24}]\}$	151.69		
$K_{12}\{(Mo_2O_2S_2)_8(OH)_{12}[N_2C_2H_4(CH_2PO_3)_4]_2\}\cdot 40H_2O$	271.62	0.95	14
$K_2H_{16}\{(Mo_2O_2S_2)_{10}(OH)_{14}[N(CH_2PO_3)_3]_4\}\cdot 60H_2O$	363.35		
$[(TeO_3)_4(Mo_2O_2S_2)_{12}(OH)_{12}(C_9H_9O_4P)_6]^{8-}$	227.47	0.95	15
$[(AsO_4)_4(Mo_2O_2S_2)_{12}(OH)_{12}(C_9H_9O_6)_4]^{12-}$	210.47		

* In some articles, water vapor adsorption capacities are reported in units of $cm^3\ g^{-1}$ (STP). Based on the conversion relationship m = 18000V/22414 , these values can be converted into mass-based units of $mg\ g^{-1}$.

14. Proton Conductivity of Representative POM-Based Conductors

Table S7 Comparison of proton conductivities and activation energies for representative POM-based crystalline materials.

Compound	Protion Conductivity (S/cm)	Temperature (℃)	RH (%)	Ref
{Mo_{12}}	**3.92×10^{-4}**	**90**	**98%**	**This work**
{Mo_{16}}	**4.53×10^{-3}**	**90**	**98%**	
$(NH_4)_{42}[Mo_{132}O_{372}(CH_3COO)_{30}(H_2O)_{72}]\cdot ca.300H_2O\cdot ca.10\cdot CH_3COONH_4$	1.07×10^{-2}	80	98%	16
$[Li(H_2O)_4]\ [\{CuI(H_2O)_{1.5}\}\{Cu^{II}(H_2O)_3\}_2\{W^{VI}_{12}O_{36}(OH)_6\}]\cdot N_2\cdot H_2S\cdot 3H_2O$	1.72×10^{-2}	80	98%	17
$[Mo_{132}O_{372}(OH)_{10}(H_2O)_{12}(SO_4)_5(CH_3COO)_{20}]^{52-}$	1.17×10^{-3}	70	98%	12
$[Sm(H_2O)_5(CO_2CH_2NH_3)_2][Al(OH)_6Mo_6O_{18}]\cdot 10H_2O$	4.53×10^{-3}	80	95%	18
$H_2[Cu_2OL_3(H_2O)_2]\ [Ce(L)(H_2O)_3(PW_{11}O_{39})]\cdot 17H_2O$	3.175×10^{-4}	85	98%	19
$H_4[CuL_3]_2[Ln(H_2O)_3(PW_{11}O_{39})]_2\cdot 28H_2O$	1.750×10^{-4}			
$NH_2(CH_3)_2]_{10}[Na_4(H_2O)_8]H_3[As_4W_{42}O_{142}(OH)_4(CH_3COO)_2Rh_3(H_2O)_4]\cdot 13H_2O_4[NH(CH_3)_2]$	1.90×10^{-4}	25	65%	20
$[PMo_{12}O_{40}][H_2PhI]_3[HPhI]\cdot 4H_2O$	2.02×10^{-4}	100	98%	21
$(NH_4)_5[Mo_8(OH)_2O_{24}(\mu_8\text{-}PO_4)]\ (H_2O)_2$	1.17×10^{-4}	80	95%	22
$(C_3N_2H_5)_{29}(NH_4)_6H_{12}[(PMo_8O_{27})_8(C_{10}P_4O_{12}N_2H_{20})_4(PO_4)_4Cs(Mo_4O_{10}(H_2O)_4)]$	9.70×10^{-3}	100	98%	23
$H_4[Co(phen)_3]_2[NaO(H_2O)(s\text{-}Mo_8O_{26})]\cdot 22H_2O$	3.06×10^{-3}	80	98%	24

15. Heating and Cooling Cycles of compound 1 and 2

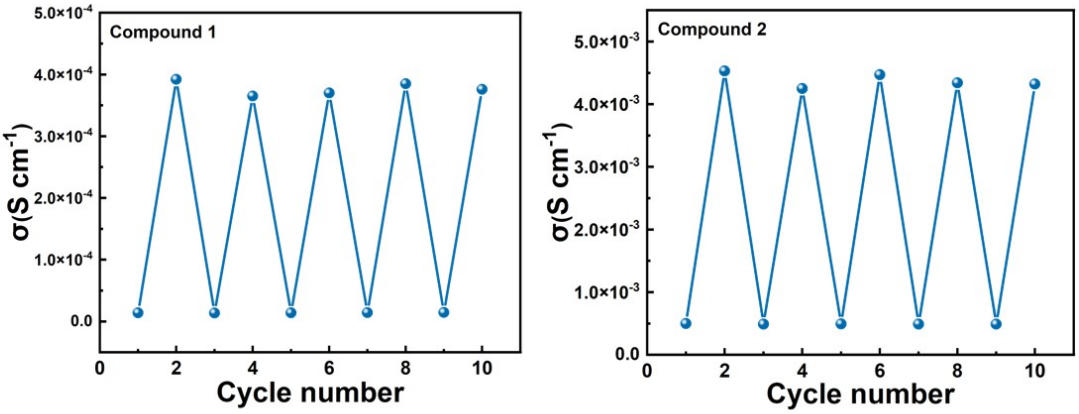

Fig. S17 Successive heating and cooling cycles of compounds 1 (left) and 2 (right) between 30 and 90 °C.

Table S8 Successive heating–cooling cycles were performed on compounds **1** and **2** over the temperature range of 30-90 °C, and the resistance (R) and proton conductivity (σ) were measured at different cycle numbers.

Compound	*Times*	*T(℃)*	*R* (Ω)	*σ* (S cm^{-1})
Compound 1	1	30	4.71×10^{4}	1.30×10^{-5}
	2	90	1.56×10^{3}	3.92×10^{-4}
	3	30	4.37×10^{4}	1.40×10^{-5}
	4	90	1.70×10^{3}	3.62×10^{-4}
	5	30	4.44×10^{4}	1.38×10^{-5}
	6	90	1.64×10^{3}	3.70×10^{-4}
	7	30	4.31×10^{4}	1.42×10^{-5}
	8	90	1.59×10^{3}	3.85×10^{-4}
	9	30	4.22×10^{4}	1.45×10^{-5}
	10	90	1.63×10^{3}	3.76×10^{-4}

	1	30	1229	4.98×10^{-4}
	2	90	135	4.53×10^{-3}
	3	30	1217	5.03×10^{-4}
	4	90	137	4.48×10^{-3}
	5	30	1234	4.96×10^{-4}
Compound 2	6	90	134	4.51×10^{-3}
	7	30	1200	5.10×10^{-4}
	8	90	136	4.50×10^{-3}
	9	30	1209	5.06×10^{-4}
	10	90	138	4.46×10^{-3}

16. FT-IR spectra of compound 1 and 2 after measurement

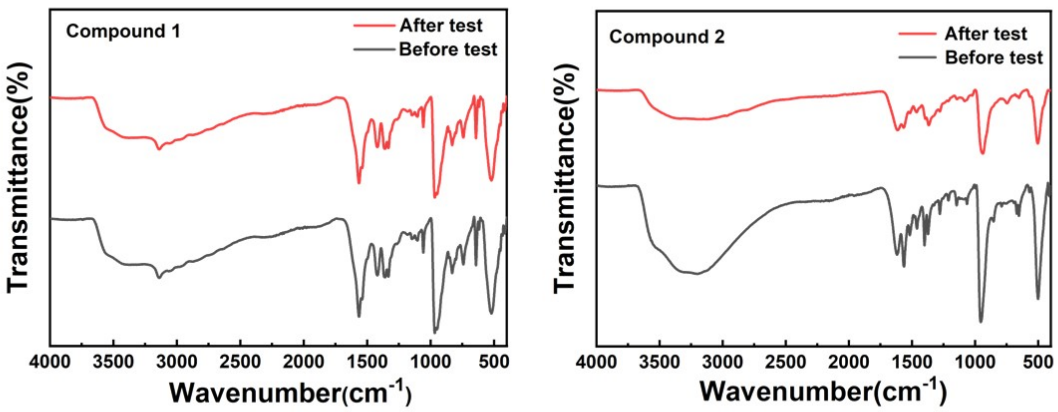

Fig. S18 FT-IR spectra of compound **1** and **2** before and after proton conduction testing.

17. PXRD spectra of compound 1 and 2 after measurement

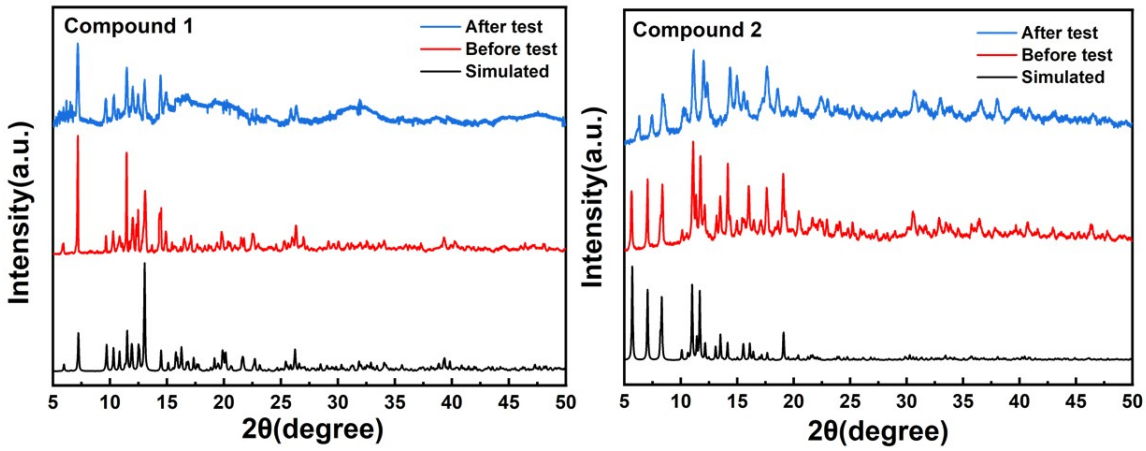

Fig. S19 PXRD spectra of compound **1** and **2** before and after proton conduction testing.

18. Calculation of BVS Value

Bond valence calculations were performed for each bond using the bond distance (R) measured and empirical parameters R_0 and B: bond valence = EXP((R_0-R)/B). BVS for each metal centre was then summed from all bond valences of the bonds listed. The parameters R_0 and B were taken from Gagne & Hawthorne[25].

Table S9. BVS results for the molybdenum atoms in compound **1**.

Atom	BVS calc. for Mo
Mo1	5.117
Mo2	5.099
Mo3	5.239
Mo4	5.052
Mo5	5.136
Mo6	5.080

Table S10. BVS results for the molybdenum atoms in compound **2**.

Atom	BVS calc. for Mo
Mo1	5.139
Mo2	5.182
Mo3	5.162
Mo4	5.136
Mo5	5.071
Mo6	5.230
Mo7	5.278
Mo8	5.270

19. Partial bond lengths

Table S11. Partial bond lengths for compound **1**.

Bond	Length/Å	Bond	Length/Å
Mo1-Mo2	2.8159(5)	Mo6-O3[1]	2.056(4)
Mo1-S1	2.3350(12)	Mo6-O7[1]	2.061(3)
Mo1-S2	2.3290(12)	Mo6-O14	1.681(4)
Mo1-O2	1.690(4)	O4-C24	1.251(7)
Mo1-O3	2.091(3)	O5-C24	1.257(6)
Mo1-O4	2.333(3)	O18-C41	1.243(7)
Mo1-O7	2.084(3)	O19-C41	1.258(7)
Mo2-S1	2.3296(12)	N16-C17	1.411(13)
Mo2-S2	2.3256(12)	N16-C20	1.308(13)
Mo2-O5	2.461(4)	N16-C21	1.434(7)
Mo2-O6	1.674(4)	N19-C18	1.343(12)
Mo2-O11	2.099(4)	N19-C20	1.336(11)
Mo2-O12	2.092(4)	C17-C18	1.358(13)
Mo3-Mo4	2.8308(6)	C21-C22	1.381(7)
Mo3-S3	2.3127(12)	C21-C23[1]	1.391(8)
Mo3-S6	2.3156(14)	C21-N16A	1.432(9)
Mo3-O1	2.051(4)	N33-C34	1.385(7)
Mo3-O8	1.679(4)	N33-C37	1.325(7)

Mo3-O13	2.078(4)	N33-C38	1.443(6)
Mo3-O26	2.474(6)	N36-C35	1.358(8)
Mo4-S3	2.3106(13)	N36-C37	1.324(7)
Mo4-S6	2.3178(13)	C22-C23	1.394(7)
Mo4-O10	1.673(4)	C23-C24	1.524(7)
Mo4-O11	2.070(4)	C34-C35	1.357(9)
Mo4-O12	2.059(4)	C38-C39	1.401(7)
Mo5-Mo6	2.8221(6)	C38-C40	1.387(7)
Mo5-S4	2.3046(13)	C39-C40[2]	1.391(7)
Mo5-S5	2.3024(15)	C39-C41	1.516(7)
Mo5-O1	2.042(4)	N16A-C17A	1.409(16)
Mo5-O9	1.677(4)	N16A-C20A	1.313(16)
Mo5-O13	2.060(4)	N19A-C18A	1.345(14)
Mo6-S4	2.3163(14)	N19A-C20A	1.333(14)
Mo6-S5	2.3109(13)	C17A-C18A	1.359(15)

[1]2-X,-Y,1-Z;[2]1-X,1-Y,-Z

Table S12. Partial bond lengths for compound **2**.

Bond	Length/Å	Bond	Length/Å
Mo5-Mo4	2.8041(13)	Mo8A-O27	1.66(2)
Mo5-S1	2.328(3)	Mo8A-O18	2.13(3)
Mo5-S3	2.336(3)	Mo8A-O26	2.14(3)
Mo5-O5	2.086(8)	Mo1-Mo8[1]	2.992(9)
Mo5-O12	1.702(8)	Mo1-S9[1]	2.282(17)
Mo5-O1	2.336(7)	Mo1-S10[1]	2.814(15)
Mo5-O4	2.081(8)	Mo1-O11	2.255(13)
Mo4-S1	2.322(3)	Mo1-O9	1.919(14)
Mo4-S3	2.340(3)	Mo1-O28	1.66(2)
Mo4-O6	2.070(8)	Mo8-S9	2.833(19)
Mo4-O3	2.096(8)	Mo8-S10	2.318(7)
Mo4-O2	2.336(7)	Mo8-O17	2.450(10)
Mo4-O14	1.690(9)	Mo8-O30	2.098(19)
Mo3-Mo2	2.8100(13)	Mo8-O29	2.07(2)
Mo3-S2	2.328(3)	Mo8-O31	1.680(17)
Mo3-S4	2.312(3)	K1-S8[2]	3.747(12)
Mo3-O6	2.087(8)	K1-S5	3.639(5)
Mo3-O3	2.108(7)	K2-K5[3]	4.367(15)
Mo3-O7	2.413(8)	K2-K6	4.777(18)
Mo3-O15	1.674(9)	K2-O38	2.13(6)
Mo2-S2	2.332(3)	K2-O25	3.389(19)
Mo2-S4	2.316(3)	K4-K4[4]	4.68(2)
Mo2-O11	2.092(8)	K4-K4[2]	4.68(2)
Mo2-O13	1.669(9)	K4-S10	3.767(19)
Mo2-O9	2.070(9)	K4-S5	3.15(2)
Mo2-O8	2.477(8)	K4-O30[2]	3.29(3)
Mo6-Mo7	2.8059(15)	K4-O30	2.74(3)
Mo6-S6	2.302(4)	K4-O31[2]	3.26(3)
Mo6-S5	2.318(3)	K5-K7[5]	4.000(12)
Mo6-O10	2.410(9)	K5-O39	3.25(4)
Mo6-O5	2.077(8)	K5-O26	3.00(3)
Mo6-O4	2.090(8)	K5-O23	3.09(2)
Mo6-O16	1.680(9)	K5-O40	3.46(3)

Mo7-Mo8	3.215(4)	K6-K7	3.58(2)
Mo7-S6	2.333(5)	K6-O32	3.30(3)
Mo7-S5	2.315(4)	K6-O29[3]	3.25(2)
Mo7-O17	2.515(11)	K7-O5	3.364(9)
Mo7-O18	2.05(3)	K7-O39	3.42(3)
Mo7-O19	1.687(11)	K7-O40	3.24(3)
Mo7-O26	2.33(3)	O2-C6	1.257(12)
Mo7-O30	2.15(2)	O1-C6	1.255(12)
Mo7-O29	2.00(2)	N1-N2	1.377(9)
Mo1A-Mo8A[1]	2.763(6)	N1-C2	1.343(12)
Mo1A-S7	2.332(15)	N1-C4	1.437(12)
Mo1A-S8[1]	1.862(13)	N2-C5	1.328(14)
Mo1A-O11	1.992(11)	N3-C2	1.335(14)
Mo1A-O9	2.232(12)	N3-C5	1.294(12)
Mo1A-O8	2.464(9)	C1-C3[1]	1.402(14)
Mo1A-O20	1.687(16)	C1-C4	1.380(14)
Mo8A-S7[1]	1.798(16)	C1-C6	1.517(13)
Mo8A-S8	2.277(11)	C3-C4	1.385(14)

[1]1-X,1-Y,1-Z;[2]1/3+Y,2/3-X+Y,2/3-Z;[3]1/3+Y,2/3-X+Y,5/3-Z;[4]1/3-Y+X,-1/3+X,2/3-Z;[5]1/3-Y+X,-1/3+X,5/3-Z

20. References

1 E. Cadot, B. Salignac, S. Halut, F. Sécheresse, *Angew. Chem. Int. Ed. Engl,* 1998, **37**, 611-613.

2 P. Ramaswamy, N. E. Wong, G. K. Shimizu, *Chem Soc Rev,* 2014, **43**, 5913-5932.

3 X. Liu, D. Zhang, L. Li, X. Sun, L. Zhang, H. Yuan, *Dalton Trans,* 2017, **46**, 9103-9109.

4 A. V. Konkova, D. V. Evtushok, N. V. Kuratieva, A. A. Ivanov, M. A. Shestopalov, *J. Cluster Sci,* 2024, **35**, 1601-1611.

5 H. Y. Zang, A. R. de la Oliva, H. N. Miras, D. L. Long, R. T. McBurney, L. Cronin, *Nat. Commun.,* 2014, **5**, 3715.

6 A. Dolbecq, E. Cadot, F. Sécheresse, *Compt. Rend. Acad. Sci. Ser. IIC, Chem,* 2000, **3**, 193-197.

7 J. F. Lemonnier, S. Floquet, J. Marrot, E. Terazzi, C. Piguet, P. Lesot, A. Pinto, E. Cadot, *Chemistry,* 2007, **13**, 3548-3557.

8 L. Deng, X. Dong, Z. H. Zhou, *Chemistry,* 2021, **27**, 9643-9653.

9 H. Y. Zang, J. J. Chen, D. L. Long, L. Cronin, H. N. Miras, *Chem Sci,* 2016, **7**, 3798-3804.

10 J. Lin, N. Li, S. Yang, M. Jia, J. Liu, X. M. Li, L. An, Q. Tian, L. Z. Dong, Y. Q. Lan, *J. Am. Chem. Soc.,* 2020, **142**, 13982-13988.

11 Z. K. Zhu, Y. Y. Lin, L. D. Lin, X. X. Li, Y. Q. Sun, S. T. Zheng, *Inorg. Chem.,* 2020, **59**, 11925-11929.

12 X. X. Li, C. H. Li, M. J. Hou, B. Zhu, W. C. Chen, C. Y. Sun, Y. Yuan, W. Guan, C. Qin, K. Z. Shao, X. L. Wang, Z. M. Su, *Nat. Commun.,* 2023, **14**, 5025.

13 Y. X. Li, S. Liu, Y. H. Fan, S. Andra, D. B. Dang, Y. M. Li, Y. Bai, *Inorg. Chem.,* 2024, **63**, 3637-3641.

14 B. Li, Y. X. Meng, Q. Q. Liu, X. Y. Chen, X. Liu, H. Y. Zang, *Chem Commun (Camb),* 2023, **59**, 13446-13449.

15 B. Li, X. Duan, Y. Cui, T. Li, X. Chen, Q. Liu, X. Liu, Y. Meng, W. Ren, L. Wang, S. Liang, H. Y. Zang, *Angew. Chem. Int. Ed. Engl.,* 2024, **63**, e202408096.

16 X. Meng, H. N. Wang, S. Y. Song, H. J. Zhang, *Chem. Soc. Rev.,* 2017, **46**, 464-480.

17 A. Ravi, R. Biswas, S. Das, S. K. Das, *J. Chem. Sci,* 2023, **136**, 3.

18 J. Miao, Y. Liu, Q. Tang, D. He, G. Yang, Z. Shi, S. Liu, Q. Wu, *Dalton Trans,* 2014, **43**, 14749-14755.

19 T. Yang, Y. Li, Z. Zhao, W. Z. Yuan, *Sci. China:Chem,* 2022, **66**, 367-387.

20 K. Kang, L. Li, M. Zhang, X. Miao, L. Lei, C. Xiao, *Inorg Chem,* 2022, **61**, 11463-11470.

21 N.-N. Ji, Z.-Q. Shi, X.-X. Xie, G. Li, *CrystEngComm,* 2020, **22**, 8161-8165.

22 E. Armakola, I. R. Salcedo, M. Bazaga-Garcia, P. Olivera-Pastor, G. Mezei, A. Cabeza, T. A. Fernandes, A. M. Kirillov, K. D. Demadis, *Inorg Chem,* 2019, **58**, 11522-11533.

23 F. Liu, J. Lin, J. Ji, Y. Na, S. Uchida, X. Fang, *Inorg Chem,* 2023, **62**, 15340-15345.

24 L. Xu, Z. Wang, Y. Lu, T. Yan, H. Tian, X. Li, S. Wang, X. Sun, Z. Zhang, T. Dang, S. Liu, *New J. Chem,* 2018, **42**, 16516-16522.

25 O. C. Gagne, F. C. Hawthorne, *Acta Crystallogr B Struct Sci Cryst Eng Mater,* 2015, **71**, 562-578.